Intelligent Robotic System with Fuzzy Learning Controller and 3D Stereo Vision

SHIUH-JER HUANG
Department of Mechanical Engineering
National Taiwan University of Science and Technology
No. 43, Keelung Road, Section 4, Taipei, 106, TAIWAN
sjhuang@mail.ntust.edu.tw http://homepage.ntust.edu.tw/sjhuang/

Abstract: - It is well known that robotic manipulators are highly nonlinear coupling dynamic systems. It is difficult to establish an appropriate mathematical model for designing a model-based controller. The model-free feature of fuzzy logic control strategy was employed to design robotic motion controller. However, there is no guide rule for designing the fuzzy rule bank and parameters, it still needs time consuming trial-and-error work for rules bank and fuzzy parameters adjustment. We had developed self-organizing fuzzy control and adaptive fuzzy sliding mode control two intelligent learning mechanism for solving this implementation problem. In addition, a low cost stereo vision system is developed on chip processor. It can be integrated into robotic system for executing visual servo robotic motion control purpose. Both systems can be constructed on Nios II SOPC developing board with ALTERA FPGA chip to manipulate a retrofitted Mitsubishi robotic system. The 3-D position information between the target and stereo vision system was extracted by stereo vision algorithm first. Then, the relative motion between the robotic end-effector and the target can be planned to guide robot arm to catch the object. The self-organizing fuzzy control and fuzzy sliding mode control algorithms are employed to monitor the trajectory motion of each joint. The experimental results show that this visual servo robotic system can track and catch a moving target in 3D space and execute some interaction functions with player.

Key-Words: - visual servo, robotic system, self-organizing fuzzy control, fuzzy sliding mode control, FPGA chip

1 Introduction

Since cameras are useful robotic sensors for the robotic automation operation in non-autonomous environment, it was first integrated with robotic system as the visual feedback control in 1979. How to integrate the machine vision into the robotic system for improving manipulator working ability is still a hot research topic in recent years [1,2]. For the mobile robot or human interaction robot, they need stereo vision to detect the environment obstacle and achieve image navigation or moving object following purposes [3]. Due to the development of semi-conductor and digital circuit design technology, the new system- on-programmable-chip (SOPC) provides fertilize functions for the servo control, image processing and network communication purposes. FPGA chips are firstly used in communication and signal processing. Recently, it has been employed in motor control [4], and the PID control of robotic arm [5]. Here, a SOPC system is employed to implement a vision servo robotic control system for human interaction function.

In addition, the accurate dynamic model for a multi-axis manipulator is difficult to establish for model based controller design and real time computation, the model-free intelligent fuzzy control schemes are adopted in the robotic motion control field [6]. However, the design of a traditional fuzzy controller depends fully on an expert or the experience of an operator to establish the fuzzy rule bank. Hence, a self-organizing fuzzy controller with learning ability was proposed in [7], new establishing processes of the fuzzy rules bank had been found for reducing the trial-and-error effort. Later, the modified learning methods for self-organizing fuzzy controller (SOFC) were proposed in [8,9] for further simplification. For each sampling instant, the output response error and error change stimulate two fuzzy subsets of their corresponding universe of discourse E and CE. Hence only four rules are modified in each sampling step. Since, this approach has learning ability to establish and regulate the fuzzy rules bank continuously, its control implementation can be started with zero initial fuzzy rules. The fuzzy rules were adjusted on-line based on a simple equation instead of a performance decision table.

ISBN: 978-1-61804-023-7

However, it is still a 2D fuzzy rules. Here, ID adaptive fuzzy sliding mode control strategy [10] is modified and employed to design the individual controller for each joint. A novel gain scheduling algorithm is introduced to modify this control algorithm for improving the overall control performance. The real-time human-robot interaction control strategies are developed for the robotic system to achieve the functions of tracking moving objects and catching them or demonstrate the real time interaction games with player.

2 Robotic System Structure

The visual servo robotic control structure with Atera Nios II embedded development kit is shown in Fig. 1. Verilog HDL (Hardware Description Language) is selected to code the hardware circuits of this visual servo robotic control system on FPGA chip. The main servo control system can be divided into FPGA internal hardware implementation and Nios II micro-processor software programs implementation two parts. The main functions of FPGA hardware circuits are motor optical encoder decoding, limit switch detecting, pulse width modulation (PWM) generating and CMOS image signal capturing. The functions of the Nios II micro-processor software programs are the communication with PC by using UART, robotic inverse kinematics calculation, robotic motion trajectory planning, robotic motion control schemes, and digital image processing algorithm. Two CMOS color image sensors with 356x292 pixels resolution are used to extract the environment time-varying change for robotic visual-based motion control. The robotic system is an old Mitsubishi Movemaster RV-M2 manipulator with a retrofitted FPGA control structure to substitute original commercial controller.

3 Trajectory planning and Inverse Kinematics

Generally, the end-effector working position or motion path in Cartesian space are converted into control variables in joint coordinates for controlling purpose by using the inverse kinematics and Denavit-Hartenberg transformation matrix. Although some efficient analysis methods had been proposed [11], they are time consuming and complicated mathematical operations. Since the chessboard and the operation range of this vision based robotic system are limited on horizontal plane, the end-effector orientation is specified as orthogonal and point down to the X-Y horizontal plane. Then the Denavit-Hartenberg transformation matrix of end-effector with respect to the reference inertia coordinate is

$$ {}^{ref}T_{tool} = {}^{0}A_1 \cdot {}^{1}A_2 \cdot {}^{2}A_3 \cdot {}^{3}A_4 \cdot {}^{4}A_5 = \begin{bmatrix} 1 & 0 & 0 & x \\ 0 & -1 & 0 & y \\ 0 & 0 & -1 & z \\ 0 & 0 & 0 & 1 \end{bmatrix} \quad (1) $$

Based on the Mitsubishi RV-M2 robot link parameters, and forward kinematics calculation, the Denavit-Hartenberg transformation matrix can be derived and described by using the robotic D-H parameters a_i and θ_i. The joint angle θ_i can be solved by comparing the D-H matrix components and some trigonometric functions operations based on following steps:

Step 1: $\theta_1 = \theta_5 = A\tan 2(p_y, p_x)$

Step 2: $b = \pm\sqrt{(x^2 + y^2)}$

Step 3: $$\theta_3 = \cos^{-1}\left(\frac{b^2 + (d_1 - d_5 - z)^2 - a_1^2 - a_1(b - a_1) - a_2^2 - a_3^2}{2a_2a_3}\right) \quad (2)$$

Step 4: $$\theta_2 = A\tan 2\frac{(a_2 + a_3C_3)(d_1 - d_5 - z) - (a_3S_3)\cdot b}{(a_2 + a_3C_3)\cdot b + a_3S_3\cdot(d_1 - d_5 - z)}$$

Step 5: $\theta_4 = -\theta_2 - \theta_3$

This approach can reduce the trigonometric functions calculation from 17 times to 7 comparing with that of traditional inverse kinematics. The computer time on the Nios II SOPC can be reduced from 4.5 ms to 2.5 ms for increasing the system closed loop frequency.

For the multi-input and multi-output system, the motion trajectory of each joint corresponding to the end-effector point to point (PTP) motion in Cartesian space need be planned to move and stop at the same time for the simultaneous motion purpose. The trapezoid speed curve with a constant acceleration and deceleration time T_a, a constant acceleration value a_m and the total motion time T, is the most popular trajectory planning for the PTP motion. There relationships are

$$a_m T_a = v_m \text{ and } T = \frac{X}{v_m} + T_a \quad (3)$$

The axis with largest angular moving range is chosen to calculate the total motion time T based on the specified maximum acceleration, a_m, and maximum velocity, v_m. Then the acceleration time and the maximum velocity of the other axes can be derived based on these moving angles, total motion time and the maximum acceleration information.

ISBN: 978-1-61804-023-7

$$T_{ai} = \frac{T}{2} - \sqrt{\frac{T^2}{4} - \frac{X_i}{a_m}} \text{ and } v_m = a_m T_{ai} \quad (4)$$

Those trajectory planning parameters of this 5 DOF robot are derived.

4 Controller Design

4.1 Self-organizing fuzzy learning controller

Generally, the system dynamic response feature can be represented as an auto-regression and moving average (ARMA) model:

$$\theta(nT) = A(q^{-1})\theta(nT-T) + Mu(nT-mT) + B(q^{-1})u(nT-mT-T)$$
$$A(q^{-1}) = a_0 + a_1 q^{-1} + \cdots + a_{r-1} q^{-(r-1)} \quad (5)$$
$$B(q^{-1}) = b_0 + b_1 q^{-1} + \cdots + b_{s-m-1} q^{-(s-m-1)}$$

where mT is the system time delay. M is the direct system forward gain for this position control system. The values of r, s and m depend on the dynamic characteristics of the control system. Due to system nonlinearity and uncertainty, they are difficult to estimate for this 5 DOF robotic system. Fortunately, fuzzy control has a model free feature. It does not require definite mathematical model and system parameters. Hence, they are not employed in the following controller design. If the system is excited with a different control input $u'(nT - mT)$ at time step $nT - mT$, there will be a new output value $\theta'(nT)$ at time step nT. The input difference, Δu, of the servo motor control voltage will cause a system joint output deviation $\Delta\theta$. If the deviations $\Delta\theta$ and $\Delta\dot{\theta}$ are small, then the relationships between control input and corresponding output deviations can be described

$$\Delta\theta = M \cdot \Delta u \text{ and } \Delta\dot{\theta} = \frac{M}{T}\Delta u \quad (6)$$

If a system at time step nT has angular output error $\Delta\theta$ and error rate $\Delta\dot{\theta}$, the theoretical corresponding control input correction values are Δu_e and Δu_{ce}, respectively.

$$\Delta u_e \equiv \frac{\Delta\theta}{M} \text{ and } \Delta u_{ce} \equiv \frac{T\Delta\dot{\theta}}{M} \quad (7)$$

Since the system has only one control input u, the control input correction must be an appropriate combination of the above two terms. In general, the following form can be chosen:

$$\Delta u = (1-\xi)\Delta u_e + \xi\Delta u_{ce} \quad (8)$$

ξ is a design parameter representing the weighting distribution between Δu_e and Δu_{ce}. If there is a large difference between the system angular output $\theta(nT)$ and desired value θ_d, an appropriate design choice is to select a value $\theta'(nT)$ between $\theta(nT)$ and θ_d. Then the system joint output θ will approach the desired value θ_d gradually with a weighting parameter γ.

$$\theta'(nT) = (1-\gamma)\theta(nT) + \gamma\theta_d,\ 0 < \gamma < 1 \quad (9)$$

Then the system output and output change deviations become

$$\Delta\theta(nT) = \gamma[\theta_d - \theta(nT)] \equiv \gamma e(nT) \quad (10)$$

$$\Delta\dot{\theta}(nT) = \gamma\dot{e}(nT) \equiv \frac{\gamma}{T}ce(nT) \quad (11)$$

From equations (6) and (10), the correction value of the control input can be represented as

$$\Delta u = \frac{\gamma}{M}[(1-\xi)e(nT) + \xi ce(nT)] \quad (12)$$

The output error, $e(nT)$, and error change, $ce(nT)$, are divided into 5 fuzzy subsets from -1 to +1 with interval 0.5. For each control step, the fuzzy input variables, i.e. the system output error and error change will stimulate two fuzzy subsets of the E and CE universe of discourse, respectively. Since the control input u is derived from the fuzzy rules inference, the rules modification will influence four fuzzy rules for each control step. The correction value of each fuzzy rule is proportional to its exciting strength w_{ij}. The excitation strength is designed as a triangular membership function and calculated with a linear interpolation algorithm. Then the new control input of the i^{th} rule is

$$\begin{aligned} u_i(nT+T) &= u_i(nT) + \Delta u_i \\ &= u_i(nT) + w_{ei}w_{cei}\frac{\gamma}{M}[(1-\xi)e(nT) + \xi ce(nT)] \end{aligned} \quad (13)$$

The term $\frac{\gamma}{M}$ in the above equation can be considered as the correction weighting. Here, M is chosen as 1 in order to eliminate the identification procedure and reduce computing time during implementation. The correction weighting is regulated by the parameter γ only. A larger value of γ will introduce a large correction of fuzzy rules and system output oscillation. This parameter only influences the transient response but not the steady state performance. According to experimental experience, this parameter can be selected as a large value (for example 0.9), and it can be adjusted to a smaller value (for example 0.3) after the learning procedure has converged. It is not crucial for this control strategy. Generally, a γ value of between 0.3 and 0.9 can achieve stable convergent SOFC

systems. The SOFC control block diagram is shown in Fig. 2.

4.2 Fuzzy Sliding Mode Joint Controller

Here the sliding mode concept is combined with fuzzy control strategy to design a model-free fuzzy sliding mode controller (FSMC) robotic motion control. In addition, the fuzzy variables gains scheduling strategy is integrated into the model-free fuzzy sliding mode control scheme for improving the transient response and steady state error performance. It is an enhanced and extended development from the original FSMC approach proposed by Huang and Lin [10] to achieve excellent performance.

A sliding surface on the phase plane is defined to specify the error converging line in pahse plane.

$$s(t) = (\frac{d}{dt} + \lambda)e_1 = e_2 + \lambda e_1 \qquad (14)$$

Where $e_i = x_{id} - x_i$ are defined as the state control errors. This sliding variable, s, will be used as the input signal for establishing a fuzzy logic control system to approximate the specified perfect control law, u_{eq}. With this perfect control law, the closed loop control system has an asymptotical stability dynamic behavior.

$$\dot{s}(t) + \lambda s(t) = 0 \qquad (15)$$

Since λ is a positive value, the sliding surface variable, s, will gradually converge to zero. Based on the definition of sliding surface variable, s, in eq. (5), the system output error will converge to zero, too. In this study, a fuzzy system is employed to approximate the mapping between the sliding variable, s, and the control law, u, instead of model-based calculation. This control law may have certain difference with the perfect control law u_{eq}, then the following equation can be derived.

$$\dot{s}(t) = -\lambda s(t) + b(X,t)[u_{eq}(t) - u(t)] \qquad (16)$$

Generally, $b(X)$ is a positive constant or a positive slow time-varying function for practical physical systems. Based on the Lyapunov theorem, the sliding surface reaching condition is $s \cdot \dot{s} < 0$. If a control input u can be chosen to satisfy this reaching condition, the control system will converge to origin of the phase plane. It can also be found that $\dot{s}$ increases as u decreases and vice versa in (16). If $s > 0$, then the increasing of u will result in $s\dot{s}$ decreasing. When the condition is $s < 0$, $s\dot{s}$ will decrease with the decreasing of u. based on this qualitative analysis, the control input u can be designed in an attempt to satisfy the inequality $s \cdot \dot{s} < 0$.

The control voltage change for each sampling step is derived from fuzzy inference and defuzzification calculation instead of the equivalent control law derived from the nominal model at the sliding surface. It can eliminate the chattering phenomenon of a traditional sliding mode control. The one dimensional fuzzy rules, Fig, 3(b), is designed based on the sliding surface reaching condition, $s \cdot \dot{s} < 0$. The sliding surface variable, s, is employed as the one dimensional fuzzy input variable.

Only eleven fuzzy rules are employed in this control system to obtain appropriate dynamic response and control accuracy. The input membership functions are scaled into the range of -1 and +1 with equal span. Hence a scaling factor gs is employed to map the sliding surface variable, s, into this universe of discourse. A scaling factor gu is employed to adjust the value of control voltage. The fuzzy sliding control block diagram and membership functions of fuzzy input and output variables, and the fuzzy rules of the FSMC are shown in Fig. 3(a) and 3(b), respectively.

The membership function used for the fuzzification is of a triangular type. The function can be expressed as

$$\mu(x) = \frac{1}{w}(-|x - a| + w) \qquad (17)$$

where w is the distribution span of the membership function, x is the fuzzy input variable and a is the parameter corresponding to the value 1 of the membership function. The height method is employed to defuzzify the fuzzy output variable for obtaining the control voltage of each joint control motor.

$$u = \frac{\sum_1^m \mu^j \cdot U^j}{\sum_1^m \mu^j} = \frac{\sum_1^m \mu^j \cdot C^j}{\sum_1^m \mu^j} \equiv \sum_1^m \phi_j C^j \qquad (18)$$

where m is the rules number and C^j is the consequent parameter. Here, eleven equal-span triangular membership functions are used for the fuzzy input variable, s, and the fuzzy output variable, u.

The divisions of this membership functions can be expanded or shrunk by changing the scaling parameter of membership functions. The gain scheduling parameter is used to map the corresponding variables into this nominal range. These mapping parameters are specified as g_S, and gu for the sliding variable and control voltage, respectively, whose values are linear functions of sliding variable with different slopes. This approach is a novel gain scheduling 1D fuzzy sliding mode control structure. The values of these parameters are

not critical they can be roughly determined by simple experimental tests.

5 Digital Image Processing and Stereo Vision

The image raw data extracted from CMOS sensor must go through certain processes to obtain useful information. The process flow chart is shown in Fig. 4. Human eye has good acuminous with respect to brightness Y and it is described as image gray signal. The image pre-processing has transformed the 8 bits image raw data of the pixel into 24 bits RGB color space data. In order to reduce the un-necessary calculation of the Nios II micro-processor, the RGB image data is converted into 8 bits gray signal by the following formula

$$\begin{bmatrix} Y \\ Cr \\ Cb \end{bmatrix} = \begin{bmatrix} 0.299 & 0.587 & 0.114 \\ -0.167 & -0.332 & 0.500 \\ 0.500 & -0.419 & -0.0813 \end{bmatrix} \begin{bmatrix} R \\ G \\ B \end{bmatrix} \quad (19)$$

Here, median filter is used to filter out the image noise by selecting the median chroma value of the pixels gray scale around a target pixel as the gray scale of this target pixel for smoothing operation. Then a histogram equalization can be used to enhance certain subjects by selecting an appropriate threshold value for the grey histograms of the image features to distinguish the object from the background. This threshold value is chosen to convert the analog image brightness signal into binary signal of each pixel. This image processing scheme is employed to identify the target location in 3D space by using 2 COMS images. Two CMOS sensors are installed with L_c relative distance in horizontal line. The coordinate origin is located in the center of two CMOS sensors, as Fig. 5. Then, the 3D object coordinates can be derived based on triangular theorem.

$$X_{Target} = \frac{\sin(\theta - \varphi)}{\sin(\theta + \varphi)} \cdot \frac{L_c}{2} \quad (20)$$

$$Z_{Target} = \frac{\sin\theta \sin\varphi}{\sin(\theta + \varphi)} \cdot L_c \quad (21)$$

$$Y_{Target} = \tan(\theta_y) \cdot Z_{Target} \quad (22)$$

Where θ_y is target viewing angle from XZ plane. Then the FPGA controller will send this coordinate information to the robotic controller for trajectory planning and control. The robotic motion controller guides the manipulator to follow and pick up the target or execute interaction behavior with player.

6 Real-Time Human-robot Interaction Control Strategy

For the human-robot interaction objective, the robotic system reaction speed in response to the player motion and the player safety should be considered. Here, player's real-time decision logic and operation processes are developed to judge the robotic reaction choice based on the target relative motion situations calculated from stereo vision system. This robotic system has basic intelligence to self judge the most appropriate interaction behavior based on the environmental change or target motion situation. The flow chart of the overall robotic interaction control strategy is shown in Fig. 6. The dynamic reaction behaviors of real-time human-robot interaction are divided into stand-by, approach object, move to the up-right of object and grasp object four modules. The corresponding action is planned for each step, for example, motion path planning and moving time specification.

When the stereo vision system has not extracted any interaction target or the target is out of the human-robot interaction area, the manipulator is stayed in the robot origin with 500mm Z axis height as the stand-by step. Since the stereo vision and robot motion control use the same FPGA processor in this hardware control structure, both actions are worked by turn. If the target is too far away from the robot hand, the manipulator motion control interval is limited to 0.5 sec in order to avoid the target go out of the stereo vision range in next visual extraction or the player waiting too long lose the interaction feeling during the approaching object step. For the safety reason during the robot approaching target step, the manipulator should not too close to the player hand. The end-effector is specified to move to the target Z axis up-right position with 40mm height before executing grasp work or moving approach. The grasping action is processed only when the target is closed to the end-effector and their relative distance in Z direction less than 50mm.

7 Experimental Results

In order to avoid the collision in the non-autonomous environment, the trajectory planning is required for the robotic motion

control, and an appropriate controller is designed to monitor the end-effector motion trajectory. Here, the fuzzy sliding mode controller was developed to control this retrofitted Mitsubishi RV-M2 five DOF robot. For investigating the system control performance, the following experiments were performed. The sampling frequency in the joint control experiments was 200 Hz. The parameters *gs* and *gu* are used to adjust the sliding variables and control input. The choice of these parameters is not sensitive to controller implementation. If these parameters are varied within 50% and 200% of the original specified values, the control system performance is not changed significantly.

7.1 Point to point (PTP) control accuracy and static object grasping

Case (A): Self-organizing fuzzy controller

The planning trajectory for the robotic end-effector is a trapezoid speed curve with a constant acceleration and deceleration for each joint and it is moving from (0, 500, 200) mm to (400, 0, 300) mm in Cartesian space with 4 sec total traveling time. The maximum angular acceleration of each joint is limited to $30^\circ/\sec^2$. The motion trajectory in Cartesian space and the position error in each coordinate axis are shown in Fig. 7. The maximum angular tracking error of each joint is less than 0.2°. The overall position trajectory tracking error is less than 2 mm. The destination steady state position error is 0.097mm.

Case (B) Fuzzy Sliding Mode controller

In order to evaluate the FSMC control performance of robotic spot welding and assembly implementations … etc, a PTP motion trajectory of the end-effector was planned first. The planning trajectory for the robotic end-effector is a trapezoid speed curve with a constant acceleration and deceleration for each joint and it is moving from (0, 400, 250) mm to (350, 0, 300) mm in Cartesian space with 4 sec total motion time. The maximum angular acceleration of each joint is limited to $35^\circ/\sec^2$. The trajectory tracking error in each coordinate axis of Cartesian space and the joints angular error histories are shown in Fig. 8. The maximum angular tracking errors of each joint is less than 0.15°. The overall position trajectory tracking error is less than 1 mm. The destination steady state position error is 0.038mm.

7.2 Human interaction and Moving target following and grasping

Case (C) Chess gobang game

In order to evaluate the dynamic response of this vision servo robotic motion control system, a gobang game is playing within a 7x9 chessboard specified in X-Y plane. The flow chart of this non-autonomous human-robot gobang game includes competitor playing turn, end-effector moves to the calculate chess piece position, robot put down the piece, end-effector grasp a piece, robot moving back to the origin and the competitor play again. Six executing pictures are shown in Fig. 9. This vision based robotic control system can run successfully in this gobang game.

Case (D) Moving target following and grasping

In order to evaluate the human-robot interaction dynamic response of this visual servo robotic motion control system, the robot end-effector is specified to follow the player finger motion and keep a 40mm height distance for safety reason. The dynamic pictures are shown in Fig. 10(a). In addition, the moving object grasping experiment is planned as the manipulator need to grasp a white small moving ball which sticks at the tip of a hand bar moving by a player. The stereo vision system is used to extract the moving target in image space and calculate the 3D coordinates with respect to the robot end-effetor. Then the robotic fuzzy sliding mode control system is employed to monitor the corresponding following and grasping process based on this visual information. The dynamic operation pictures are shown in Fig. 10 (b).

5 Conclusion

A stereo visual servo control SOPC structure is implemented on a retrofitted 5 DOF robot for motion control and human-robot interaction games. The self-organizing fuzzy controller and fuzzy sliding mode controller with 1D fuzzy rule only were coded inside the FPGA chip for each joint motion control of this robot. This control strategy establishes the appropriate fuzzy rules bank by continuous learning instead of by trial-and-error process to simplify the implementation difficulty of a fuzzy controller. The fuzzy rules table can be initialized as zero. The feature of the proposed SOFC structure is that four rules are modified only by learning for each sampling interval instead of all rules bank. It can reduce the computing time and data base. 1D FSMC is a simple control algorithm

ISBN: 978-1-61804-023-7

and easy to implement on the on-board FPGA control structure. The experimental results show that this visual guided robotic intelligent control system can effectively and accurately monitor the robotic end-effector to track planning trajectories, extract the moving target relative distance in image space and guide robotic system to grasp the moving target and execute some interaction actions with player. This SOPC control structure can be employed in a flexible non-autonomous environment for executing random assembly or pick-and-place, collision avoidance and mobile robot visual guided operations.

Acknowledgement

This research is supported by the National Science Council under the contract NSC 99-2221-E011-021 –MY2 .

References:

[1] J. Blasco; N. Aleixos; J.M. Roger; G. Rabatel; E. Molto, “Automation and Emerging Technologies: Robotic Weed Control using Machine Vision,”Biosystems Engineering Vol. 83, Issue: 2, pp. 149-157, October, 2002.

[2] Chern-Sheng Lin; Li-Wen Lue, “An image system for fast positioning and accuracy inspection of ball grid array boards,” Microelectronics Reliability Vol. 41, Issue: 1, pp. 119-128, January 2001.

[3] Han, S.-H., Seo, W. H., Yoon, K. S., and Lee, M.-H., “Real-Time Control of an Industrial Robot Using Image-Based Visual Servoing,” Proceedings of the 1999 IEEE/RSJ International Conference on Intelligent Robots and Systems, pp. 1762-1796, 1999.

[4] F. J. Lin, D. H. Wang and P. K. Huang, “FPGA-based Fuzzy Sliding-mode Contrp; for a Linear Induction Motor Drive,” Proceedings of the IEEE Int. Conf. on Electrical Power Application, Vol. 152, No. 5, pp. 1137-11148, Sept. 2005.

[5] Y. S. Kung and G. S. Shu, “Development of a FPGA-based Motion Control IC for Robot Arm,” Proceedings of the IEEE Int. Conf. on Industrial Technology, pp. 1397-1402, 2005.

[6] Shiuh-Jer Huang and Ji-Shin Lee, “A Stable Self-organizing Fuzzy Controller for Robotic Motion Control,” IEEE Transaction on Industrial Electronics, Vol. 47, No. 2, pp. 421-428, 2000.

[7] Procky T. J. and Mamdani E. H., “A linguistic self-organizing process controller,” Automatica, Vol. 15, pp. 15-30, 1979.

[8] Zhang B. S. and Edmunds J. M., “Self-organizing fuzzy logic controller,” IEE Proceedings-D, Vol. 139, No. 5, pp. 460-464, 1992.

[9] Shao S., “Fuzzy self-organizing controller and its application for dynamic processes,” Fuzzy Sets System, Vol. 26, pp. 151-164, 1988.

[10] Shiuh-Jer Huang and Wei-Cheng Lin, 2003, “Adaptive Fuzzy Controller with Sliding Surface for Vehicle Suspension Control,” IEEE Transactions on Fuzzy Systems, Vol. 11, No. 4, pp. 550-559.

[11] L.T. Wang and C.C. Chen, “A Combined optimization Method for Solving the Inverse Kinematics Problem of Mechanical Manipulator,” IEEE Trans. On Robotics and Automation Vol.7, N0.4, 1991.

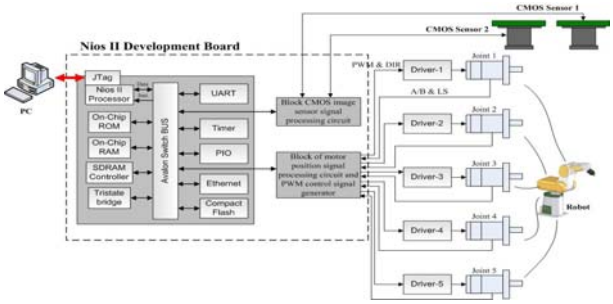

Fig. 1 SOPC Robotic control system structure.

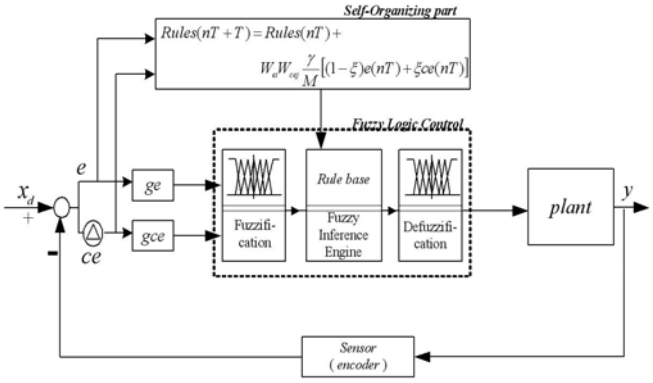

Fig.2Self-organizing fuzzy controller block diagram.

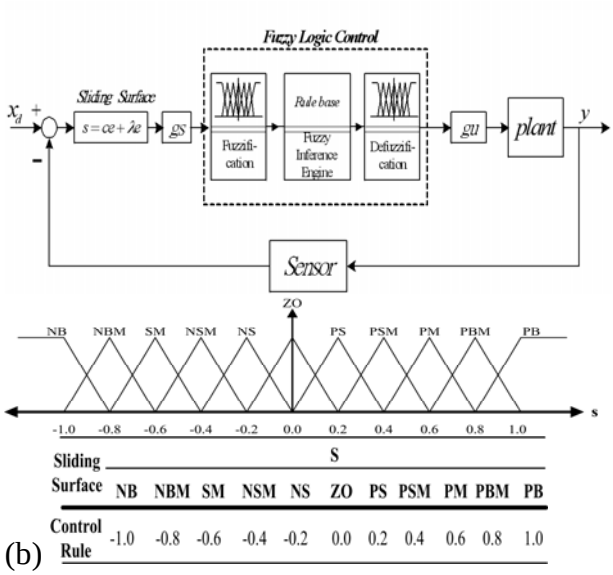

(b)

Fig. 3 (a) Fuzzy sliding mode control block diagram and (b) membership function of sliding variable and 1D fuzzy rules. .

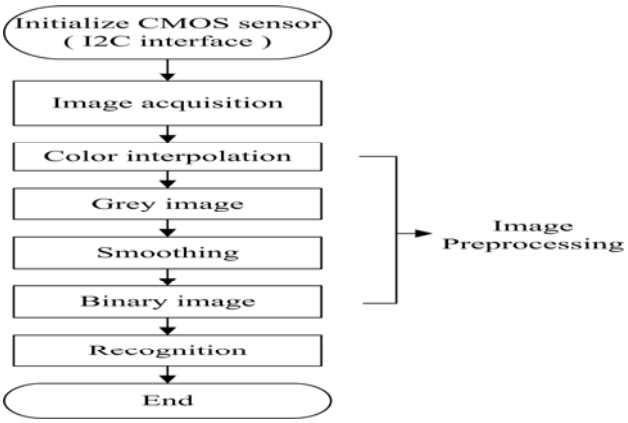

Fig. 4 Image processing flow chart.

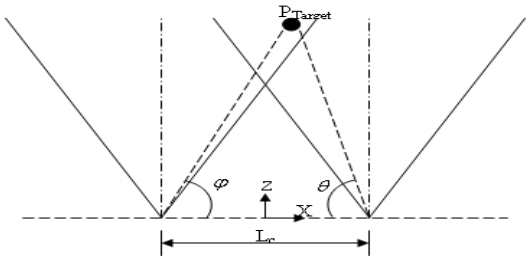

Fig. 5 Geometric relation between two CMOS sensor and target.

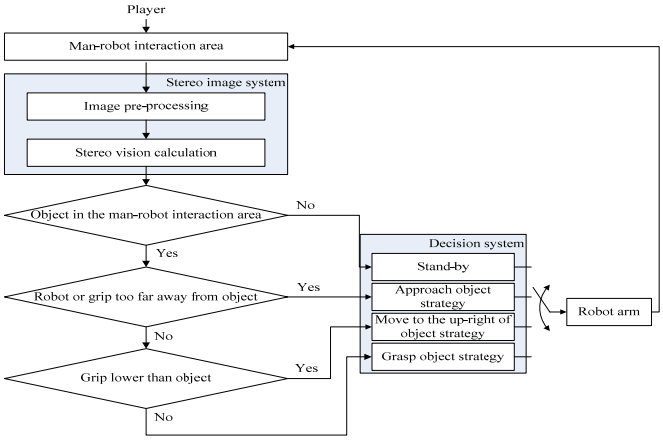

Fig. 6 The overall human-robot interaction control strategy and flow chart.

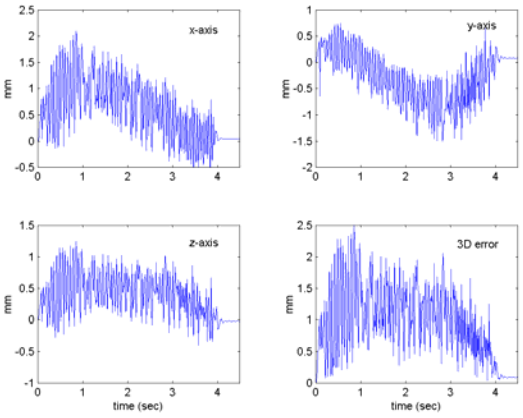

Fig. 7 SOFC Position tracking error in each axis and 3D path error.

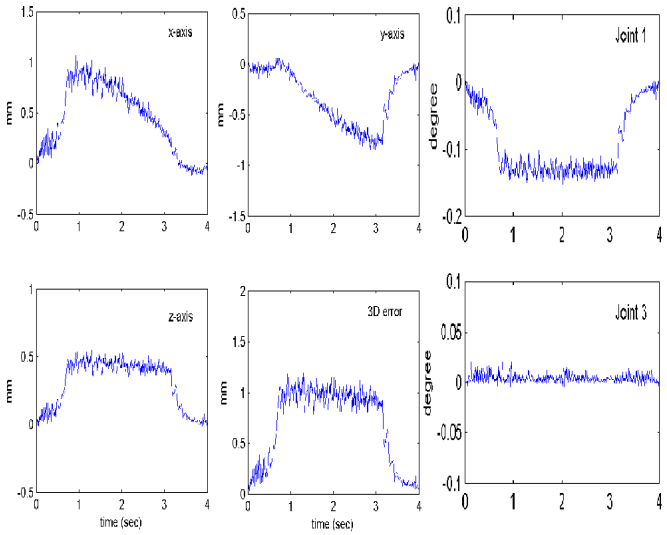

Fig. 8 The trajectory tracking error in each coordinate axis of Cartesian space and the joints angular error histories

Fig. 9 Robotic gobang game executing pictures.

Fig. 10 (a) Robot end-effector follows the moving of player finger and (b) grasp a ball.

ISBN: 978-1-61804-023-7